SUPPORTING INFORMATION

A GRAPPA algorithm for arbitrary 2D/3D non-Cartesian sampling trajectories with rapid calibration

Tianrui Luo | Douglas C. Noll | Jeffrey A. Fessler | Jon-Fredrik Nielsen

1 | CALIBRATION BOUNDARY CONDITION: CIRCULANT VS TRIMMED

Fig. S1 examines the influence of adopting circulant ACS boundary conditions on 2D reconstruction quality. In general, with proper Tikhonov regularization, the circulant boundary assumption produces similar reconstruction error as conventional ("trimmed") boundaries. The g-factor behavior is more complicated: depending on the choice of regularization parameter λ, circulant boundaries can do either slightly better or slightly worse than trimmed boundaries. In this comparison, reconstruction error with $\lambda = 5 \times 10^{-7}$ is low and difference is small between circulant and trimmed boundary conditions. This λ represents a compromise between g-factor and image/k-space error. We used this value throughout our experiments in the main text.

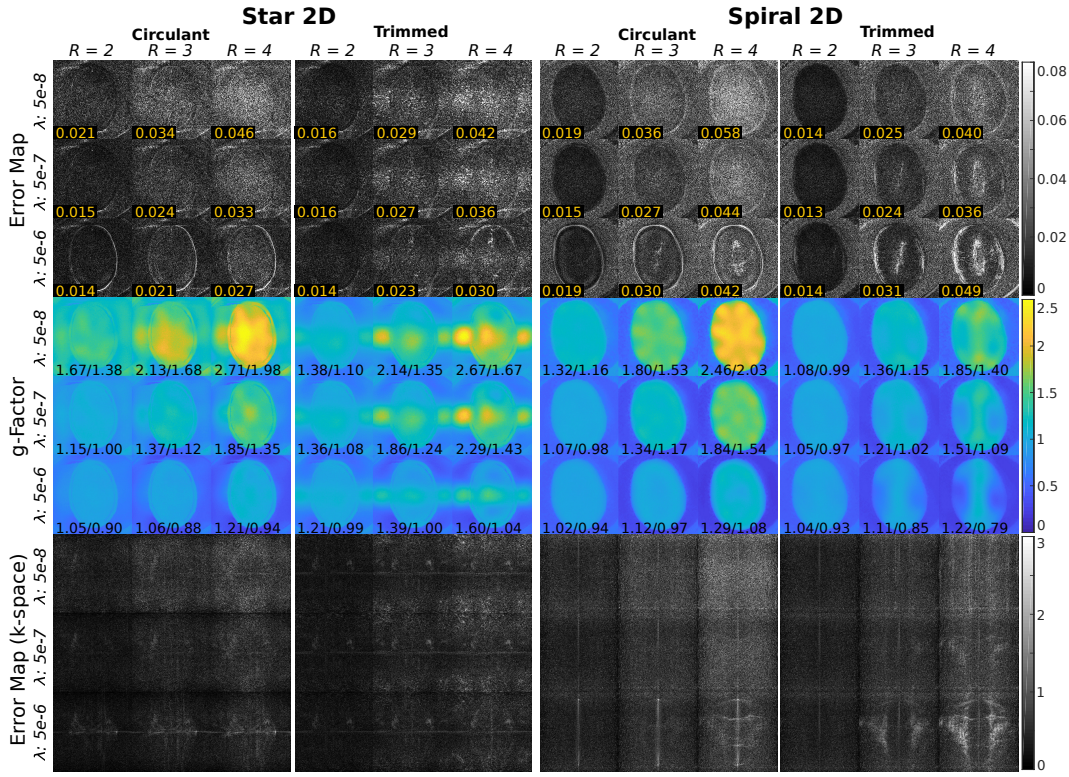

FIGURE S1 Reconstruction quality comparison of our non-Cartesian GRAPPA method using different ACS boundary conditions (circulant and trimmed), for 2D star (left panels) and spiral (right panels) datasets. The top row plots the absolute error maps and the digits are their averages within the object support. The center row plots the g-factor maps and the digits are their max/average g-factors within the support. The bottom row plots the absolute error viewed from k-space. We observe that circulant boundaries can produce similar reconstruction error as trimmed boundaries. Moreover, for certain Tikhonov regularization setups, circulant boundary outperforms trimmed boundaries.

2 | G-FACTOR FOR SENSE WITH OVER-SAMPLED CENTER OF K-SPACE

Oversampling, which occurs often near the k-space center for non-Cartesian acquisitions, is a key reason why the g-factor can fall below 1 for SENSE. To see this, consider a simple 2-pixel example with two noise-uncorrelated coil sensitivities of [1, 0.5] and [0.3, 1], respectively. For the "fully sampled" acquisition, we sample three times at k=0, and once at k=1; for the "under-sampled" acquisition, we sample once at both k=0 and k=1. The acceleration factor, R, in this example is thus 2. Following the definition of g-factor, a simple calculation would yield $g = \sqrt{3/4} < 1$.

For a more realistic example, in Fig. S2 we simulate a sampling pattern where the phase-encoding direction is over-sampled by a factor of 4.1 near the k-space center. The sensitivity maps are estimated from an *in vivo* data set; a low-resolution (64×64) matrix size is chosen to enable direct calculation. In this sampling pattern, “full”-sampling consists of both blue and red locations, while under-sampling only contains the blue locations. Again, we observe that g falls below 1 in some parts of the analytically calculated g-factor map. In summary, we conclude that oversampling, which is common for general non-Cartesian sampling, can cause the g-factor to fall below 1.

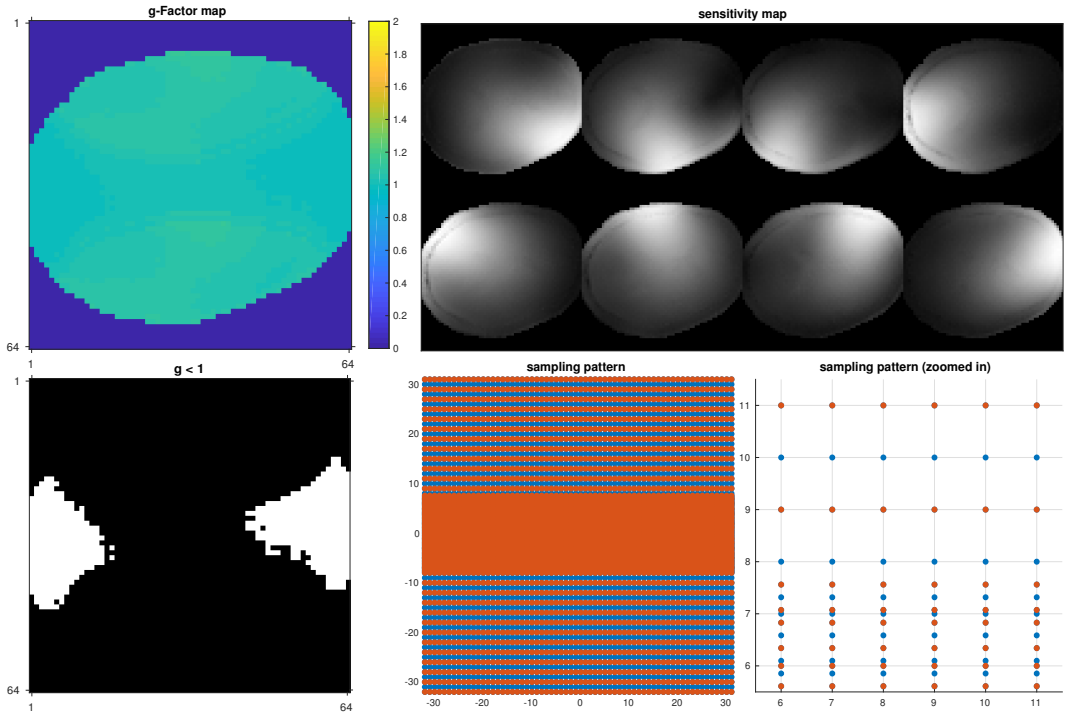

FIGURE S2 An illustration of a reconstruction with g-factor smaller than one (in some regions of the image), using realistic (*in vivo*) sensitivity maps. Here, "full" sampling consists of both blue and red locations, while "under-sampling" only contains the blue locations. The central k-space region is oversampled, as is typically the case in non-Cartesian acquisitions. The center k-space oversampling ratio 4.1 in this example produces off-grid sampling. In this example, the g-factor is just below 1.0 near the right and left parts of the image (white regions in the binary black/white image on the lower left).

3 | GRAPPA CALIBRATION USING ACS WITH DIFFERENT CONTRAST

Talagala *et al* observed that GRAPPA kernels calibrated with one acquisition can faithfully reconstruct other datasets of possibly different contrasts and resolution configurations (Ref. [13] of the maintext). This protocol can be useful for dynamic imaging, e.g., fMRI, where a structural dataset is commonly acquired alongside a number of functional activity datasets. To evaluate the use of an ACS dataset with contrast different from the to-be-reconstructed (undersampled) images, we tested reconstructing a finger-tapping dataset with kernels calibrated using a separate structural dataset. The fMRI results are shown in Fig. 7 of the main text. Here, we again show the results from Fig 7, but in addition we also show fMRI activation maps obtained with the proposed method based on ACS data from the structural dataset. The acquisition parameters are included in the **Experiments** section of the main text, and are repeated here for convenience: "…on the same subject from the fMRI experiment at the identical FOV, we also acquired a fully-sampled stack-of-spiral-out dataset with a different contrast: This acquisition still have 20 k_z platters, each containing 9 interleaves. Its other parameters are: TR=30ms, TE=2.17ms, flip-angle 8°, image matrix size $220 \times 220 \times 20$. Again, the experiments were conducted on a GE 3T scanner using an 8-channel receive-only head coil…"

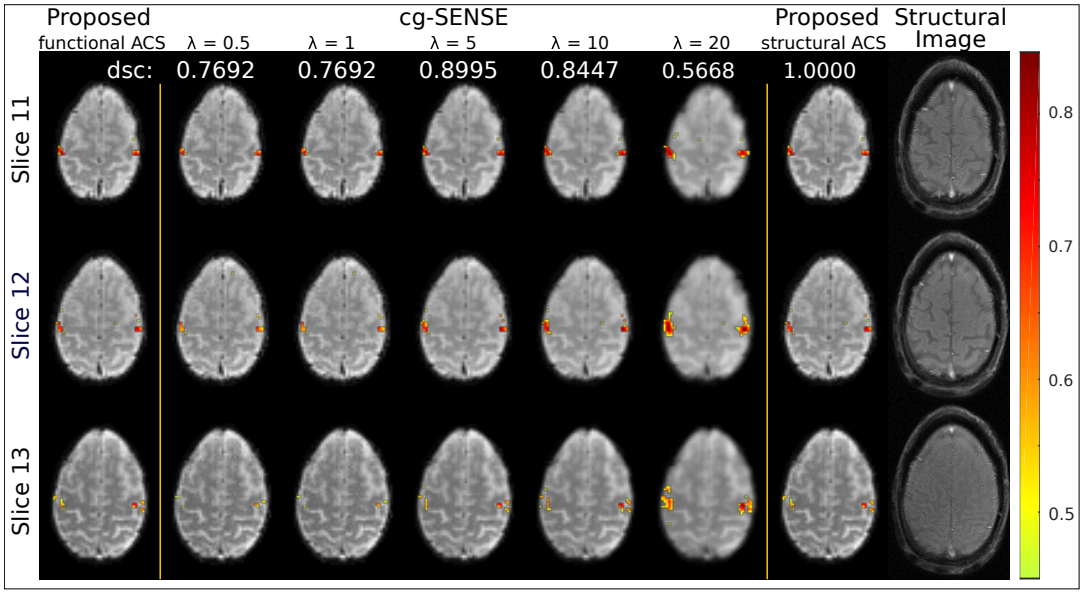

FIGURE S3 Reconstruction quality demonstration of GRAPPA kernel calibrated with ACS of a different contrast. Dice coefficients (dsc) are labeled for convenience of assessment. This figure is the same as Fig. 7, except with two extra columns (from left two right): Proposed non-Cartesian GRAPPA with kernels calibrated using the structural imaging ACS dataset; The high-resolution *structural* image of the same subject, acquired along with the fMRI scanning.